THE JOURNAL OF BIOLOGICAL CHEMISTRY VOL. 287, NO. 30, pp. 25353–25360, July 20, 2012

Live Imaging Reveals Differing Roles of Macrophages and Neutrophils during Zebrafish Tail Fin Regeneration*[S]

Received for publication, February 2, 2012, and in revised form, April 30, 2012 Published, JBC Papers in Press, May 9, 2012, DOI 10.1074/jbc.M112.349126

Li Li[‡§], **Bo Yan**[§], **Yu-Qian Shi**[§], **Wen-Qing Zhang**[¶1], **and Zi-Long Wen**[§2]

From the [‡]*Key Laboratory of Freshwater Fish Reproduction and Development, Ministry of Education, State Key Laboratory Breeding Base of Eco-Environments and Bio-Resources of the Three Gorges Area, School of Life Science, Southwest University, Chongqing 400715, China, the* [¶]*Key Laboratory of Zebrafish Modeling and Drug Screening for Human Diseases of Guangdong Higher Education Institutes, Department of Cell Biology, Southern Medical University, Guangzhou 510515, China, and the* [§]*State Key Laboratory of Molecular Neuroscience, Division of Life Science, Hong Kong University of Science and Technology, Clear Water Bay, Kowloon, Hong Kong 999077, China*

Background: Macrophages and neutrophils are key phagocytes in regeneration.
Results: Neutrophils are the primary phagocytes in the inflammatory stage and are dispensable for zebrafish fin regeneration, whereas macrophages mainly function in the resolution stage and are required for fin regeneration.
Conclusion: Macrophages and neutrophils behave differently during zebrafish fin injury and regeneration.
Significance: Our study documents that macrophages and neutrophils play distinct functions in tissue regeneration.

Macrophages and neutrophils are the pivotal immune phagocytes that enter the wound after tissue injury to remove the cell debris and invaded microorganisms, which presumably facilitate the regrowth of injured tissues. Taking advantage of the regeneration abilities of zebrafish and the newly generated leukocyte-specific zebrafish lines with labeling of both leukocyte lineages, we assessed the behaviors and functions of neutrophils and macrophages during tail fin regeneration. Live imaging showed that within 6 hours post amputation, the inflammatory stage, neutrophils were the primary cells scavenging apoptotic bodies and small cell debris, although they had limited phagocytic capacity and quickly underwent apoptosis. From 6 hours post amputation on, the resolution and regeneration stage, macrophages became the dominant scavengers, efficiently resolving inflammation and facilitating tissue remodeling and regrowth. Ablation of macrophages but not neutrophils severely impaired the inflammatory resolution and tissue regeneration, resulting in the formation of large vacuoles in the regenerated fins. In contrast, removal of neutrophils slightly accelerates the regrowth of injured fin. Our study documents the differing behaviors and functions of macrophages and neutrophils during tissue regeneration.

Successful epimorphic regeneration is essential to restore the integrity and function of injured organs (1). During this process, the immune cells play indispensable protective roles for removing dead cells, preventing invasion of microorganisms, and supporting regrowth of damaged tissues (2). Neutrophils and macrophages are two major immune system cells that participate in this process (3). Neutrophils are the first immune cells to arrive at the sites of injury, where they mainly fight against foreign invaders, such as harmful microbes, whereas macrophages emerge later and are thought to participate not only in the removal of dead cells and microbes in the wound but also the remodeling and regeneration of injured tissue (3–9). Nevertheless, despite extensive studies in the past decades (3), the *in vivo* behavior and function of each type of phagocyte and the communication between them during tissue injury and tissue regeneration are not fully characterized.

Zebrafish have recently emerged as a prominent model organism for the study of tissue regeneration due to their genetic manipulability and potent regeneration ability (10–13). The epimorphic regeneration of tail fin in larva fish is one of the well established tissue regeneration assays (10, 13). Upon tail fin amputation, the wound region undergoes a lesion-induced contraction caused by actin-purse string formation. Shortly after, the epithelium cells cover the lesion to seal the stump surface. From 12 hours post amputation (hpa)[3] on, the wound begins to regrow, and the blastema-like cells emerge under the well packed epithelium layer, signifying the regeneration of the injured tail fin. The full recovery of the wound normally requires only 4–5 days and recapitulates the process of tail fin regeneration in adult fish (10). Thus, the larva tail fin regeneration is an ideal system for studying the roles of immune cells in injury-induced tissue regeneration. Moreover, the creations of myeloid lineage-marking transgenic lines (14–16) and myeloid-defective fish (17) have provided unique opportunities to explore the actions of myeloid leukocytes during epimorphic regeneration in a living organism. However, zebrafish lines in

* This work was supported by Research Grants Council of the Hong Kong Special Administrative Region General Research Fund Grants 663109 and HKUST6/CRF/09, National Basic Research Program of China Grant 2012CB945102, and National Natural Science Foundation of China Grants 31171403 and 30828020.
[S] This article contains supplemental Figs. 1–3 and Movies 1–3.
[1] To whom correspondence may be addressed. Tel./Fax: 86-20-61647050; E-mail: zzwwqq@smu.edu.cn.
[2] To whom correspondence may be addressed. Tel.: 852-2358-7294; Fax: 852-2358-1552; E-mail: zilong@ust.hk.

[3] The abbreviations used are: hpa, hours post amputation; dpa, day(s) post-amputation; eGFP, enhanced GFP; hpf, hour(s) postfertilization; dpf, day(s) postfertilization; AO, acrine orange; MO, morpholino-oligonucleotides; morphant, MO-injected embryo; pH3, phosphohistone 3; DIC, differential interference contrast; WISH, whole mount *in situ* hybridization.

which both macrophage and neutrophil lineages are labeled by fluorescent proteins are still limited.

CORONIN 1a, also known as p57 or TACO, is an actin-binding protein that belongs to the CORONIN family (18, 19). Unlike other family members, Coronin 1a RNA is specifically synthesized by leukocytes (20). It has been suggested that Coronin 1a plays an important role in the migration, phagosome formation, and vesicle trafficking of macrophages and neutrophils (21–23). During macrophage phagocytosis, CORONIN 1a rapidly expresses on the leading edge of the lamellipodia and transiently concentrates on the early phagosome, and it quickly disappears when the phagosome is matured or fused with the lysosome (23), suggesting that CORONIN 1a is involved in the formation of phagosome. Intriguingly, continual expression of CORONIN 1a in the phagosome prevents the delivery of mycobacteria from the phagosome to the lysosomes, resulting in the enhancement of mycobacteria survival in macrophages (21). On the other hand, CORONIN 1a in neutrophils is mainly functioned in the chemotaxis (22). Similar to that in mammals, *coronin1a* (*coro1a*) in zebrafish is highly enriched in leukocytes, especially in myeloid cells and T lymphocytes, from the early development stage (24). These studies suggest that *coro1a* may serve as a marker for the full repertoire of myeloid cells in zebrafish.

In this study, the promoter region of *coro1a* was isolated and utilized to create a stable transgenic line, *Tg(coro1a:eGFP)*, in which both macrophages and neutrophils were marked by fluorescent protein in developing zebrafish embryos. Using a double transgenic line, *Tg(coro1a:eGFP;lyz:Dsred)*, in which macrophages and neutrophils could be distinguished by green and red fluorescence, respectively, combined with morpholino-induced ablation of macrophages and neutrophil-defective mutant *runx1*^{w84x}, the *in vivo* functions of macrophages and neutrophils during the epimorphic regeneration of tail fin were analyzed. Live recordings revealed that neutrophils were the major players during the inflammatory stage immediately after tail fin amputation, when they actively engulfed small dead cell debris, but appeared to have an inhibitory role in subsequent regeneration of the fin, whereas macrophages were critical for resolving inflammation and supporting normal regrowth of the regenerating tail fin. This report systematically describes the different functions of macrophages and neutrophils during the process of epimorphic regeneration of the zebrafish tail fin after amputation, and our findings provide clues for further study of the molecules involved.

EXPERIMENTAL PROCEDURES

Fish Lines—Wild-type AB, *Tg(lyz:Dsred)* (16), *Tg(coro1a:eGFP)hkz04t*, *Tg(coro1a:eGFP)hkz05t*, and *runx1*^{w84x} fish strains were maintained as described (25).

In Vitro Synthesis of Antisense RNA Probe and WISH—The *coro1a* antisense RNA probe was prepared by *in vitro* transcription according to the standard protocol. The WISH was performed as described previously (26).

Double Fluorescence Immunohistochemistry Staining—Immunohistochemistry was performed as described previously (27). To examine the co-staining of GFP and DsRed, embryos were first stained with goat anti-GFP and rabbit anti-DsRed antibody (1:250, 4 °C, overnight) and subsequently visualized by Alexa Fluor 488 donkey anti-goat (1:400, 4 °C, overnight) and Alexa Fluor 555 donkey anti-rabbit (1:400, 4 °C, overnight). Similar methods were used for co-staining of GFP and Lcp protein and of GFP and phosphohistone 3 (pH3) (28). Anti-Lcp and anti-pH3 (Upstate) antibody was visualized by Alexa Fluor donkey anti-rabbit 555 (1:400, 4 °C, overnight) (Molecular Probes).

Video-enhanced DIC Imaging—Video-enhanced DIC microscopy was performed as described (28).

Generation of Tg(coro1a:eGFP) and Tg(coro1a:eGFP; lyz:Dsred) Transgenic Lines—7.03-kb DNA sequence upstream of the *coro1a* translation start site amplified with the primers 5′-AGCAACAACGTTCTAAGAGA-3′/5′-GATGACCTGAGGAAAGACA-3′ was used as a promoter to drive eGFP expression in the pTol2 vector. The pTol2-*coro1a-eGFP* construct was injected into the wild-type (WT) fish embryos at one-cell stage. The embryos with an appropriate GFP expression were selected and raised to adults. Two founder lines *Tg(coro1a:eGFP)hkz04t* and *Tg(coro1a:eGFP)hkz05t* were identified based on their eGFP expression pattern. *Tg(coro1a:eGFP;lyz:Dsred)* double transgenic line was generated by mating F1 *Tg(coro1a:eGFP)* with *Tg(lyz:Dsred)* fish.

Fluorescence-activated Cell Sorting (FACS) and Giemsa Staining—The FACS analysis to isolate GFP-positive cells and Giemsa staining were performed as described previously (29, 30). About 300 *Tg(coro1a:eGFP)* embryos were used for FACS for each developmental stage and were repeated twice.

Live Image Analysis—The injured fish embryos were anesthetized and mounted in 1% agarose and subsequently imaged under an Olympus confocal microscope (×20 objective) for around 48 h. Images were taken every 3 min, extracted, and converted to the movie using FV10-ASW 1.7 software. Photoshop 6.0 was employed to analyze the moving trace of macrophages and neutrophils.

Acridine Orange (AO) Staining—AO staining was performed as described (31). Embryos of different stages were incubated with 5 μg/ml AO in egg water for 30 min. After washing for 1 h, the embryos were observed under the confocal microscope.

Irf8 (Interferon Regulatory Factor 8) Morpholino-oligonucleotide (MO) Injection—0.6 mM *irf8* MOsp (5′-AATGTTTCGCTTACTTTGAAAATGG-3′) or 0.3 mM *irf8* MOatg (5′-TCAGTCTGCGACCGCCCGAGTTCAT-3′) and control morpholino-oligonucleotide were injected into the one-cell stage embryos (28).

Statistical Methods—The calculated data were recorded and analyzed by Excel software. Student's *t* test was mainly used as the statistical method.

RESULTS

Tg(coro1a:eGFP) Fish Mark both Macrophages and Neutrophils—To generate zebrafish in which both macrophages and neutrophils can be marked by fluorescent protein, we isolated a 7.03-kb DNA fragment upstream of the *coro1a* translation start site and fused it with the enhanced green fluorescent protein (eGFP) gene. When this reporter construct pTol2-*coro1a-eGFP* was transiently injected into one-cell stage wild-type embryos, it displayed a typical myeloid lineage expression pattern (data not shown), suggesting that this

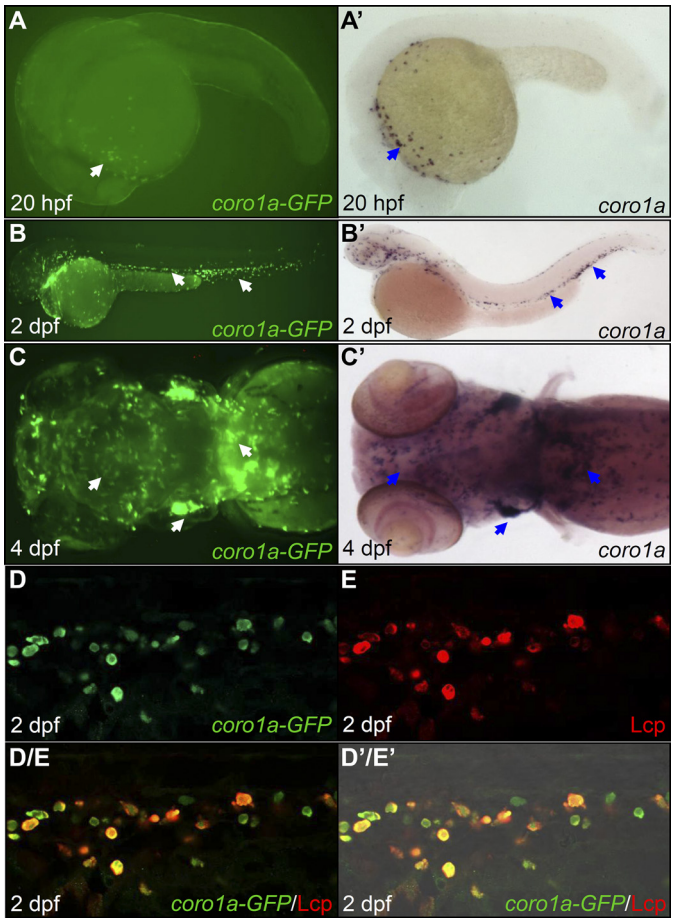

FIGURE 1. ***Tg(coro1a:eGFP)* marks both macrophages and neutrophils.** *A–C*, fluorescence imaging shows GFP signals in live *Tg(coro1a:eGFP)* embryos ($n = 40/40$) in the yolk sac at 20 hpf (*A*); in the AGM, the CHT, and the circulation at 2 dpf (*B*); and in the thymus, the kidney, and the brain at 4 dpf (*C*). *A′–C′*, WISH reveals *coro1a* RNA expression in the yolk sac at 20 hpf ($n = 40/40$) (*A′*); in the AGM, the CHT, and the circulation at 2 dpf ($n = 40/40$) (*B′*); and in the thymus, the kidney, and the brain at 4 dpf ($n = 40/40$) (*C′*). *White arrows* in *A–C* indicate the GPF^+ cells, whereas *blue arrows* in *A′–C′* represent WISH signals. *D* and *E*, GFP and Lcp double antibody staining shows the co-localization of *coro1a*-GFP and Lcp in the CHT of 2 dpf *Tg(coro1a:eGFP)* embryos ($n = 31/31$). *D/E*, *superimposed image* of *D* and *E*. *D′/E′*, *merged view* of *D/E* with the DIC image, *AGM*, aorta-gonad-mesonephros; *CHT*, caudal hematopoietic tissue.

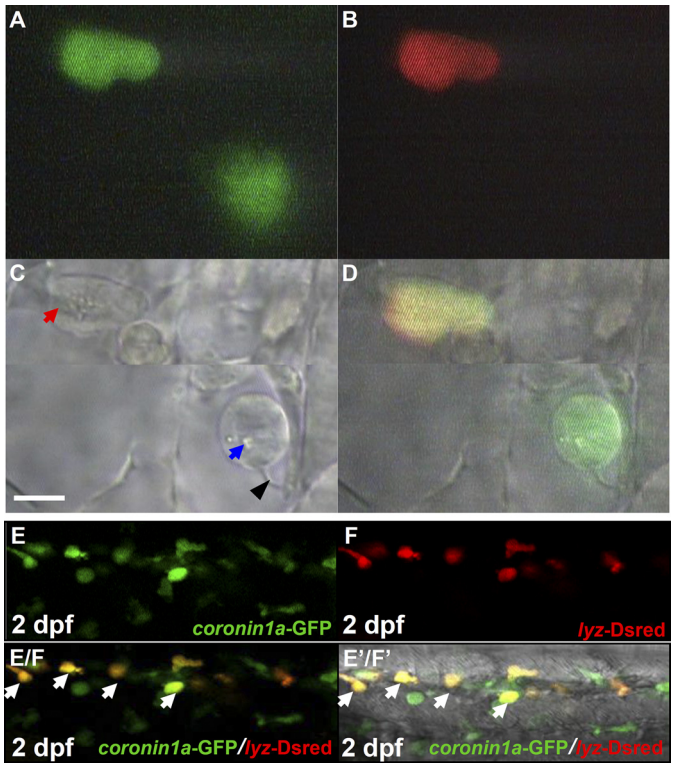

FIGURE 2. ***Tg(coro1a:eGFP;lyz:Dsred)* distinct macrophages and neutrophils.** *A–C*, live imaging (×60) of two GFP^+ cells in 2 dpf *Tg(coro1a:eGFP;lyz:Dsred)* embryos under a video-enhanced DIC microscope at the GFP channel (*A*), Dsred channel (*B*), and bright field (*BF*) channel (*C*) ($n = 12/12$). *D*, *superimposed image* of *A*, *B*, and *C*. The *blue arrow* and *black arrowhead* in *C* indicate the lysosome/phagosome inside the macrophage and the long filopodia of macrophage, respectively. The *red arrow* in *C* represents granules in neutrophils. *Scale bar*, 5 μm. *E* and *F*, confocal fluorescence imaging (×40) of the CHT region in 2 dpf *Tg(coro1a:eGFP;lyz:Dsred)* live embryos ($n = 40/40$) using the GFP (*E*) and Dsred channel (*F*), respectively. *E/F*, *superimposed image* of *E* and *F*. *E′/F′*, *merged view* of *E/F* with the DIC image. *White arrows* in *E/F* and *E′/F′* represent yellow neutrophils resulting from the merge of GFP and Dsred.

7.03-kb upstream sequence is sufficient to direct GFP expression in myeloid cells. Two independent stable transgenic lines, *Tg(coro1a:eGFP)hkz04t* and *Tg(coro1a:eGFP)hkz05t*, were recovered. Detailed characterization of both transgenic lines revealed that *coro1a-GFP* expression recapitulated the pattern of endogenous *coro1a*, which predominantly expresses in myeloid cells and T lymphocytes (24). As shown in Fig. 1, in *Tg(coro1a:eGFP)* fish (*Tg(coro1a:eGFP)hkz04t* will be used hereafter), GFP was first detected as early as 20 hours post fertilization (hpf) in myeloid cells dispersed in the yolk sac (Fig. 1*A*, *white arrow*, $n = 40/40$). As the embryos developed, the GFP-positive (GFP^+) cells were evident in the trunk, the tail region (Fig. 1*B*, *white arrows*, $n = 40/40$), the central nervous system (presumably representing microglia-specialized macrophages (31), the thymus, and the kidneys (Fig. 1*C*, *white arrows*, $n = 40/40$). The co-localization of GFP with Lcp, a pan-myeloid marker (32), in 2 day post fertilization (dpf) *Tg(coro1a:eGFP)* embryos (Fig. 1, *D–D′/E′*, $n = 31/31$) suggests that GFP marks both macrophages and neutrophils. To confirm that this is indeed the case, we performed video-enhanced DIC imaging analysis, which distinguishes macrophages from neutrophils based on their morphological appearances (33, 34). Examination of 2 dpf live *Tg(coro1a:eGFP)* embryos revealed that neutrophils defined as cells with mobile cytoplasmic granules (Fig. 2, *A*, *C*, and *D*, *red arrow*, $n = 12/12$) and macrophages defined as cells with lysosomes/phagosomes and long filopodia but a lack of cytoplasmic granules (Fig. 2, *A*, *C*, and *D*, *blue arrow* and *black arrowhead*, $n = 12/12$) were positive for GFP. From these observations, we conclude that GFP marks both macrophages and neutrophils in *Tg(coro1a:eGFP)* embryos.

The Cellular Development of Embryonic Macrophages and Neutrophils—The early *coro1a-eGFP* expression in myeloid cells in *Tg(coro1a:eGFP)* transgenic lines prompted us to define the development stages of embryonic myeloid cells. The GFP^+ cells from *Tg(coro1a:eGFP)* embryos were isolated at various developmental time points by FACS and subjected to cytological analysis. Giemsa staining revealed that at 20 hpf, all of the GFP^+ cells uniformly had a round morphology with large nuclei and scant basophilic cytoplasm (supplemental Fig. 1, *A* and *G*, $n \geq 300$), a characteristic of myeloid progenitors (35). By 24 hpf, a majority (~67%) of the GFP^+ cells remained as mye-

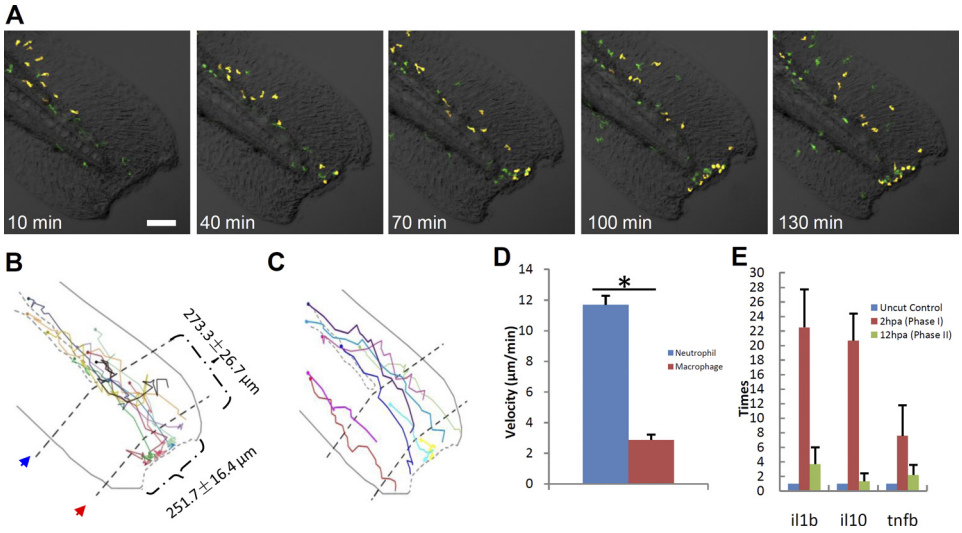

FIGURE 3. **Neutrophil and macrophage behavior upon fin transaction.** *A*, frames of different time points following tail transaction in a 72 hpf *Tg(coro1a:eGFP;lyz:Dsred)* embryo (*green*, macrophages; *yellow*, neutrophils). *Scale bar*, 100 μm. *B* and *C*, schematic diagrams show the wound size and cell migration trajectory of the first 10 neutrophils (*B*) and nine macrophages (*C*) to arrive at the wound, followed for 5 h after tail transaction. The *circle* in the end of each trajectory line represents the initial site of each myeloid phagocyte. The *red arrow* indicates the first line near the cut edge, which is the end of the notochord, and the *blue arrow* represents the second line, which is the end of circulation. The *dotted curved lines* in *B* and *C* represent vessels. *D*, histogram reveals that the velocity of neutrophils is much faster than macrophages during the process toward the wound edge ($n \geq 9$, mean ± S.E. (*error bars*)). *, statistical differences with corresponding control (*t* test, $p < 0.05$). *E*, histogram showing that the RNA level of cytokines increased dramatically in inflammatory stage but decreased thereafter until the regeneration stage ($n = 42$).

loid progenitors. However, about 14% of the GFP$^+$ cells harbored beanlike nuclei and a bubbled contour (supplemental Fig. 1*B*, $n \geq 300$), which is similar to the young macrophage reported previously (33, 36), and around 19% of the GFP$^+$ cells developed into functional macrophages defined as cells with large cytoplasmic vacuoles and some of the vacuoles loaded with dead debris (supplemental Fig. 1*C*, $n \geq 300$). No typical neutrophils were detected at this stage. At 2 dpf, in addition to the myeloid progenitors (~48%) and monocyte/macrophage lineage (~34%) (supplemental Fig. 1, *E* and *G*, $n \geq 300$), neutrophils (~17%) with the typical segmented nuclear lobes were discernible (supplemental Fig. 1, *D* and *G*, $n \geq 300$). This result is consistent with the previous studies showing that the functional monocytes/macrophages emerged at around 24 hpf (33, 36) and maturing neutrophils were not detected until 36 hpf (34). Notably, the dendritic-like cells (less than 1%) characterized by the typical dendritic filaments (37) were also detected at 2 dpf (supplemental Fig. 1*G*, $n \geq 300$), and the dendritic-like cells increased to about 1–2% at 3 dpf and displayed a more arborized morphology (supplemental Fig. 1*F*, $n \geq 300$).

Neutrophils Are the Primary Scavengers during Inflammation Stage after Tail Fin Amputation—The capability of *Tg(coro1a:eGFP)* marking both macrophages and neutrophils but *Tg(lyz:Dsred)* (16) marking only neutrophils at the embryonic stage provides an ideal system to directly assess the behaviors and functions of macrophages and neutrophils simultaneously. To achieve this, we outcrossed *Tg(coro1a:eGFP)* fish with *Tg(lyz:Dsred)*. In the double transgenic line *Tg(coro1a:eGFP;lyz:Dsred)*, neutrophils co-expressed *lyz-Dsred* and *coro1a-GFP* (*lyz*$^+$/*coro1a*$^+$) and displayed yellow fluorescence, whereas macrophages expressed *coro1a-GFP* (*coro1a*$^+$) only and displayed green fluorescence (Fig. 2, *E–E′/F′*, $n = 40/40$). To study the real-time actions of macrophages and neutrophils in tissue regeneration, the well established tail fin regeneration assay (14, 15, 38, 39) was employed in 72 hpf *Tg(coro1a:eGFP;lyz:Dsred)* embryos, making a lesion 251.7 ± 16.4 μm in length and 273.3 ± 26.7 μm from the end of the circulation (Fig. 3*B*, $n = 13$). The injured embryos were immediately viewed under a confocal microscope at 3-min intervals for 48 h. Results showed that, similar what was noted in the previous reports (14, 15), both types of myeloid cells responded immediately, but they migrated into the wound at different speeds (Fig. 3, *A–D*, $n \geq 9$; supplemental Movie 1, $n = 3$). Although a few localized resident macrophages were activated and migrated toward the lesion (Fig. 3*A*), neutrophils, with a higher mobility (Fig. 3*D*, $n \geq 9$; supplemental Movie 1, $n = 3$), were the first phagocytes to arrive at the wound, and they functioned as the major scavengers within 6 hpa (Fig. 5*L*, $n \geq 13$), during which time the inflammatory cytokines were increased to their maximum levels (Fig. 3*E*, $n = 42$). This period was thus referred to as the inflammatory stage (3, 9).

In the initial phase of the inflammatory stage, a substantial number of cells died near the edge of the wound, most of which underwent fragmentation, a characteristic of necrosis (Fig. 4, *B–D*, *white arrowhead* and *blue arrow*, $n = 13$), leading to retraction of the cut edge of the tail fin (Fig. 5*K*, $n \geq 15$). Incubation of the wounded embryos with AO (31) showed that more than half of the cell debris were vacuolar cell debris that were negative for AO (Fig. 4, *B–D*, *blue arrow*, $n = 13$), whereas others were particulate cell debris positive for AO (Fig. 4, *B–D*, *white arrowhead*, $n = 13$). Shortly after the injury, neutrophils infiltrated the wound and began to engulf both vacuolar and particulate cell debris up to a size of 0.94 ± 0.09 μm (Fig. 4, *B–D*, $n = 13$; supplemental Movie 2, $n = 5$). The phagocytotic ability of neutrophils was limited, and one neutrophil could engulf less than four pieces of cell debris (Fig. 4*G*, $n = 12$). About 20 min later, these neutrophils changed from amoeboid appearance to round shape and subsequently underwent a

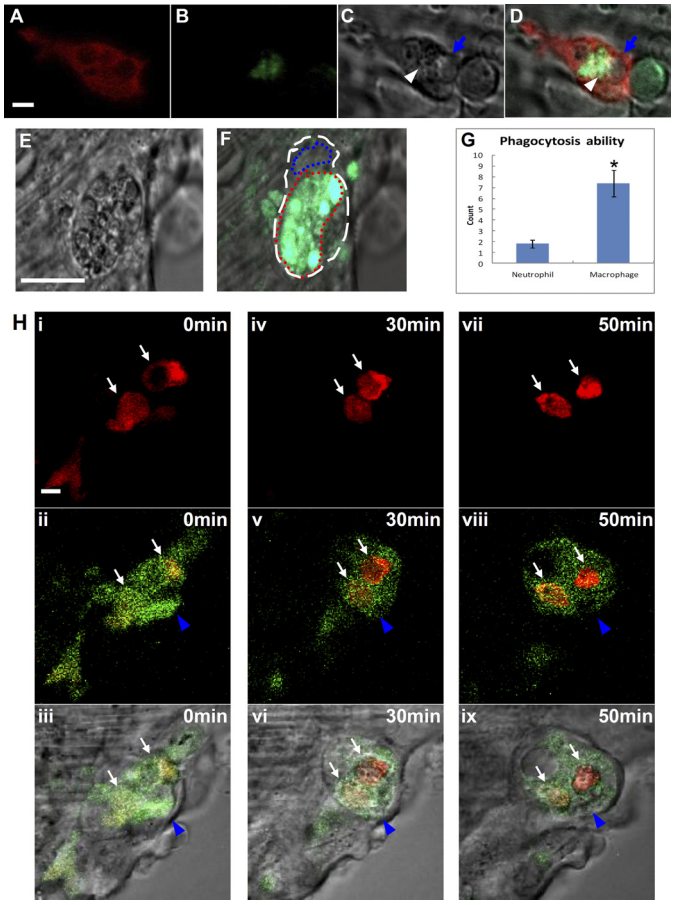

FIGURE 4. **Macrophages and neutrophils behaviors in the wound after amputation.** *A–D*, live imaging (×40) shows that *lyz*$^+$ neutrophils engulf both AO$^+$ particle cell debris and AO$^-$ vacuolar cell debris at 2 hpa ($n = 13$). The *white arrowhead* and *blue arrow* indicate the AO$^+$ particle and AO$^-$ vacuolar cell debris, respectively. *Scale bar*, 1 μm. *E* and *F*, live imaging (×40) reveals a macrophage with a large amount of cell debris (*E*, $n = 12$), including AO$^+$ particles (*green*) (*F*, $n = 12$). The *white* and *blue dashed lines* indicate the shape and the nucleus of macrophage, respectively, whereas the *red dashed line* manifests the large vacuole full of ingested debris. *Scale bar*, 10 μm. *G*, histogram reveals the phagocytosis ability (represented by the number of dead particles ingested) of macrophages and neutrophils ($n = 12$, mean ± S.E. (*error bars*)). The *asterisk* in *G* indicates statistical differences with corresponding control (*t* test, $p < 0.05$). *H*, frames (×100) of different time points of two neutrophils (indicated by *white arrows*) engulfed by a macrophage (represented by *blue arrowheads*) in a 72 hpf *Tg(coro1a:eGFP;lyz:Dsred)* embryo ($n = 7$). The *bottom panels* are merges of DIC with the *middle panels*. *Scale bar*, 1 μm.

series of morphological alterations that resembled the characteristics of apoptosis, including membrane blebbing, chromatin condensation, and nuclear fragmentation (supplemental Fig. 2*A*, $n = 7$; supplemental Movie 2, $n = 5$) (40–42). The apoptotic neutrophils, in which the engulfed cell debris was usually not fully digested, were subsequently removed by the infiltrated macrophages (Fig. 4*H*, $n = 7$).

Macrophages Emerge Later in the Wound and Are Essential for Regeneration of the Injured Tail Fin—From 6 hpa onward, macrophages became the dominant myeloid cells at the wound site (Fig. 5*L*, $n \geq 13$). Immediately after their arrival, macrophages, usually with a beanlike morphology (supplemental Fig. 2*C*, $n = 13$), displayed professional phagocytosis. An activated macrophage could engulf more than six pieces of large cell debris (0.8–3.2 μm) (Fig. 4, *E–G*, $n = 12$), including the apoptotic neutrophils (Fig. 4*H*, $n = 7$). As a consequence, the number of AO$^+$ apoptotic bodies (Fig. 5*I*, $n \geq 15$) and the number of neutrophils (Fig. 5*L*, $n \geq 13$) in the wound were rapidly reduced, and so were the levels of inflammatory cytokines (Fig. 3*E*, $n = 42$). This process, referred to as the resolution stage, lasted for 5–6 h.

To the end of the resolution stage (~12 hpa), cells in the wound began to proliferate, signifying the initiation of regeneration (Fig. 5*J*, $n \geq 10$). During the regeneration stage, the wound surface became smoother (supplemental Fig. 2, *B* and *D*, $n = 13$), and the cells around the site of amputation proliferated extensively (Fig. 5*J*, $n \geq 10$). The regeneration process continued for 4–5 days (Fig. 5, *J*, $n \geq 10$ and *K*, $n \geq 15$). During this stage, macrophages were the predominant phagocytes in the wound; they were concentrated along the growing edge and displayed a long and thin morphology (supplemental Fig. 2, *B–F*, $n = 13$ and Fig. 5*L*, $n \geq 13$).

The continuing invigilation of macrophages in the growing edge during the regeneration stage and the findings that macrophages are essential for muscle regeneration in mice (4) prompted us to speculate that macrophages might play a crucial role in the remodeling and the regrowth of the zebrafish tail fin. To support this hypothesis, we depleted macrophages by knocking down *irf8* (interferon regulatory factor 8) in zebrafish by specific MOs (28). In the *irf8* MO-injected embryos (morphants), neutrophils responded normally to tail amputation (supplemental Fig. 3, *A* and *B* and supplemental Movie 3, $n = 7$) and effectively phagocytized the small dead cell debris (supplemental Fig. 3, *D–F*, $n = 11$). However, macrophages were hardly seen in the *irf8* morphants (supplemental Fig. 3*C*, $n = 15$). As a result, the removal of cell debris was delayed in the *irf8* morphants (Fig. 5*I*, $n \geq 15$). Likewise, the cell proliferation and growth rate of the regenerating tail fin in the *irf8* morphants were significantly reduced compared with that in controls (Fig. 5, *J*, $n \geq 10$ and *K*, $n \geq 15$). Although the injured tail was eventually regrown in the *irf8* morphants, the regenerated fin formed large vacuoles (Fig. 5, *A*, *B*, *E*, and *F*, $n \geq 11$). These vacuoles emerged at 3 dpa with 82 ± 23 μm in length, and by 5 dpa, some of the vacuoles enlarged to 103 ± 48 μm in length (Fig. 5*F*, $n = 4/11$). In contrast, the tail fin regeneration in the homozygous *runx1*^{w84x} mutant embryos (25), in which neutrophils but not macrophages are significantly reduced (43), was normal (Fig. 5, *D* and *H*, $n \geq 6$). Unexpectedly, the regeneration speed in the *runx1*^{w84x} mutants was slightly accelerated (Fig. 5*N*, $n \geq 6$), reflected by the increased cell proliferation and faster growth of the injured fin in mutant embryos compared with that in siblings (Fig. 5, *M* and *N*, $n \geq 6$), suggesting that neutrophils have a negative effect on fin regeneration. From these observations, we conclude that macrophages are essential for the regeneration of zebrafish tail fin, whereas neutrophils appear to have an inhibitory role.

DISCUSSION

In the present study, we created a *Tg(coro1a:eGFP)* transgenic line in which the GFP reporter is driven by a 7.03-kb *coro1a* regulatory sequence. We demonstrated that *coro1a-GFP* expressed in myeloid cells (macrophages, neutrophils, and dendritic-like cells) and lymphocytes in early development (Fig.

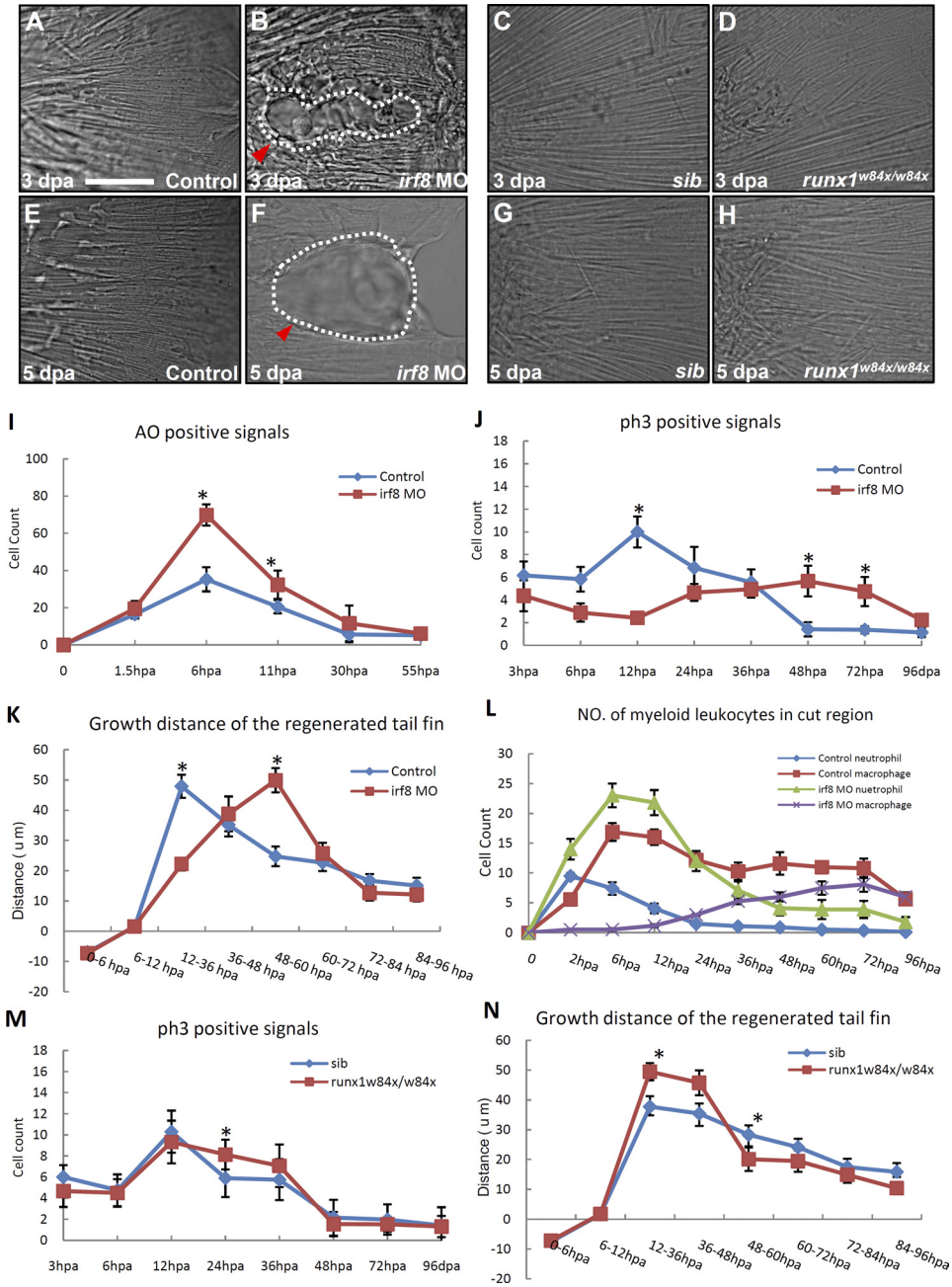

FIGURE 5. **Macrophages and neutrophils play different roles in the regeneration of tail fin.** *A–H*, DIC images show the morphology of newly regenerated fin in 3 dpa control ($n = 20/20$) (*A*), 3 dpa *irf8* morphants ($n = 6/11$) (*B*), 3 dpa siblings (*sib*) ($n = 12/12$) (*C*), 3 dpa *runx1*^{w84x} mutant ($n = 7/7$) (*D*), 5 dpa control ($n = 20/20$) (*E*), 5 dpa *irf8* morphants ($n = 4/11$) (*F*), 5 dpa siblings ($n = 11/11$) (*G*), and 5 dpa *runx1*^{w84x} mutants ($n = 6/6$) (*H*). *Scale bar*, 50 μm. The *white dashed lines* in *B* and *F* indicate the outline of the vacuoles (*red arrowheads*). *I*, histogram reveals the number of pieces of AO$^+$ cell debris at different time points after the transaction of tail fin in 72 hpf control ($n \geq 15$, mean $\pm$ S.E. (*error bars*)) and *irf8* morphants ($n \geq 16$, mean $\pm$ S.E.) *Tg(coro1a:eGFP;lyz:Dsred)* embryos. *J*, histogram reveals the number of pH3$^+$ cells at different time points after the transaction of tail fin in 72 hpf control ($n \geq 10$, mean $\pm$ S.E.) and *irf8* morphants ($n \geq 10$, mean $\pm$ S.E.) *Tg(coro1a:eGFP;lyz:Dsred)* embryos. *K*, histogram quantifies the grow distance (μm) of regenerated fin at different stages after transaction in 72 hpf control ($n \geq 17$, mean $\pm$ S.E.) and *irf8* morphants ($n \geq 15$, mean $\pm$ S.E.) *Tg(coro1a:eGFP;lyz:Dsred)* embryos. *L*, histogram reveals the number of myeloid phagocytes in the wound at different time points after transaction of tail fin in 72 hpf control ($n \geq 13$, mean $\pm$ S.E.) and *irf8* morphants ($n \geq 14$, mean $\pm$ S.E.) *Tg(coro1a:eGFP;lyz:Dsred)* embryos. *M*, histogram reveals the number of pH3$^+$ cells at different time points after the transaction of tail fin in 72 hpf sibling ($n \geq 11$, mean $\pm$ S.E.) and *runx1*^{w84x} mutant ($n \geq 6$, mean $\pm$ S.E.) embryos. *N*, histogram quantifies the grow distance (μm) of regenerated fin at different stages after transaction in 72 hpf sibling ($n \geq 11$, mean $\pm$ S.E.) and *runx1*^{w84x} mutant ($n \geq 6$, mean $\pm$ S.E.) embryos. The *asterisks* in *I–K*, *M*, and *N* indicate statistical differences with corresponding control (*t* test, $p < 0.05$).

1) as well as in adulthood (data not shown). To our knowledge, this is the first zebrafish reporter line that marks all of the leukocytes. The early expression of GFP in *Tg(coro1a:eGFP)* transgenic fish allows us to isolate embryonic myeloid cells for cytological analysis. Giemsa staining of *coro1a*$^+$ cells shows that functional monocytes/macrophages emerge early at 24 hpf, whereas mature neutrophils are evident until 2 dpf (supplemental Fig. 1). Notably, a small number of dendritic-like cells, which have an arborized morphology and dendritic filaments, are also detected from 2 dpf onward (supplemental Fig. 1). This result is consistent with previous studies using molecular markers and functional analysis (33, 36).

By utilizing the *Tg(coro1a:eGFP;lyz:Dsred)* double transgenic lines, the *in vivo* behaviors and functions of macrophages and neutrophils in the larva tail fin regeneration (14, 15, 38, 39) were directly assayed in a living embryo. We showed that upon injury, the local resident macrophages and neutrophils (Fig. 3*A* and supplemental Movie 1) were the first phagocytes to be activated. Shortly after, distant/circulation-derived neutrophils were recruited to the wound, and finally the macrophages distant from the lesion or monocytes in the circulation arrived. The consequential colonization of the wound by the local resident macrophages/neutrophils, distant/circulation-recruited neutrophils, and distant/circulation-derived macrophages is partially in agreement with the previous study in mice, which suggested that the local resident macrophages may facilitate the activation and recruitment of the distant/circulation-derived neutrophils and macrophages (44). However, contrary to this notion, our study showed that the activation and recruitment of both local resident and distant/circulation neutrophils are not affected in the *irf8* morphants, in which resident macrophages and circulating monocytes are absent (28), indicating that the local resident macrophages are not essential for the activation and recruitment of distant/circulation-derived neutrophils. Further study is needed to clarify the role of the local resident macrophages.

In the inflammation stage during the first several hours after fin amputation, neutrophils are the first group of cells that reach the wound, and they are the predominant functional phagocytes during this stage, suggesting the conservational response process of myeloid cells after injury (9). In addition to removing micro-organisms (45), we show that neutrophils can engulf cell debris during tissue damage, suggesting that neutrophils are also involved in the resolution of inflammation and perhaps subsequent tissue regeneration as suggested previously (9, 45, 46). Unexpectedly, we found that the regeneration speed of the fin is slightly faster in the neutrophil-deficient *runx1*^{w84x} (44) (Fig. 5), indicating that neutrophils may play an inhibitory role in the regeneration stage. This result is consistent with the previous findings in mice, in which the depletion of neutrophils leads to faster epidermal healing when measured by wound closure (3, 46). It will be of great interest to investigate how neutrophils inhibit the tissue regeneration in general.

In the resolution and regeneration stages, macrophages appear to be dominant effect cells to remove large cell debris as well as apoptotic neutrophils, demonstrating that macrophages but not neutrophils are the key scavengers for resolving inflammation and facilitating tissue regrowth. Consistent with previous studies in mice (4, 7), we further document that the depletion of macrophages in zebrafish leads to the delay of the clearance of cell debris, decrease of regeneration speed, and formation of vacuoles in the regenerating fin. Further investigation is required for elucidating the underlying mechanisms.

Acknowledgment—We thank Dr. Phil Crosier for providing the Tg(lyz:Dsred) transgenic line.

REFERENCES

1. Poss, K. D., Keating, M. T., and Nechiporuk, A. (2003) Tales of regeneration in zebrafish. *Dev. Dyn.* **226,** 202–210
2. Medzhitov, R. (2007) Recognition of microorganisms and activation of the immune response. *Nature* **449,** 819–826
3. Martin, P., and Leibovich, S. J. (2005) Inflammatory cells during wound repair. The good, the bad, and the ugly. *Trends Cell Biol.* **15,** 599–607
4. Arnold, L., Henry, A., Poron, F., Baba-Amer, Y., van Rooijen, N., Plonquet, A., Gherardi, R. K., and Chazaud, B. (2007) Inflammatory monocytes recruited after skeletal muscle injury switch into antiinflammatory macrophages to support myogenesis. *J. Exp. Med.* **204,** 1057–1069
5. Leibovich, S. J., and Ross, R. (1975) The role of the macrophage in wound repair. A study with hydrocortisone and antimacrophage serum. *Am. J. Pathol.* **78,** 71–100
6. Leibovich, S. J., and Ross, R. (1976) A macrophage-dependent factor that stimulates the proliferation of fibroblasts *in vitro*. *Am. J. Pathol.* **84,** 501–514
7. London, A., Itskovich, E., Benhar, I., Kalchenko, V., Mack, M., Jung, S., and Schwartz, M. (2011) Neuroprotection and progenitor cell renewal in the injured adult murine retina requires healing monocyte-derived macrophages. *J. Exp. Med.* **208,** 23–39
8. Rappolee, D. A., Mark, D., Banda, M. J., and Werb, Z. (1988) Wound macrophages express TGF-α and other growth factors *in vivo*. Analysis by mRNA phenotyping. *Science* **241,** 708–712
9. Serhan, C. N., Brain, S. D., Buckley, C. D., Gilroy, D. W., Haslett, C., O'Neill, L. A., Perretti, M., Rossi, A. G., and Wallace, J. L. (2007) Resolution of inflammation. State of the art, definitions, and terms. *FASEB J.* **21,** 325–332
10. Kawakami, A., Fukazawa, T., and Takeda, H. (2004) Early fin primordia of zebrafish larvae regenerate by a similar growth control mechanism with adult regeneration. *Dev. Dyn.* **231,** 693–699
11. Poss, K. D., Shen, J., Nechiporuk, A., McMahon, G., Thisse, B., Thisse, C., and Keating, M. T. (2000) Roles for Fgf signaling during zebrafish fin regeneration. *Dev. Biol.* **222,** 347–358
12. Poss, K. D., Wilson, L. G., and Keating, M. T. (2002) Heart regeneration in zebrafish. *Science* **298,** 2188–2190
13. Yoshinari, N., Ishida, T., Kudo, A., and Kawakami, A. (2009) Gene expression and functional analysis of zebrafish larval fin fold regeneration. *Dev. Biol.* **325,** 71–81
14. Ellett, F., Pase, L., Hayman, J. W., Andrianopoulos, A., and Lieschke, G. J. (2011) *mpeg1* promoter transgenes direct macrophage-lineage expression in zebrafish. *Blood* **117,** e49–56
15. Gray, C., Loynes, C. A., Whyte, M. K., Crossman, D. C., Renshaw, S. A., and Chico, T. J. (2011) Simultaneous intravital imaging of macrophage and neutrophil behavior during inflammation using a novel transgenic zebrafish. *Thromb. Haemost.* **105,** 811–819
16. Hall, C., Flores, M. V., Storm, T., Crosier, K., and Crosier, P. (2007) The zebrafish lysozyme C promoter drives myeloid-specific expression in transgenic fish. *BMC Dev. Biol.* **7,** 42
17. Hogan, B. M., Layton, J. E., Pyati, U. J., Nutt, S. L., Hayman, J. W., Varma, S., Heath, J. K., Kimelman, D., and Lieschke, G. J. (2006) Specification of the primitive myeloid precursor pool requires signaling through Alk8 in zebrafish. *Curr. Biol.* **16,** 506–511
18. de Hostos, E. L. (1999) The coronin family of actin-associated proteins. *Trends Cell Biol.* **9,** 345–350
19. Uetrecht, A. C., and Bear, J. E. (2006) Coronins. The return of the crown. *Trends Cell Biol.* **16,** 421–426
20. Gatfield, J., Albrecht, I., Zanolari, B., Steinmetz, M. O., and Pieters, J. (2005) Association of the leukocyte plasma membrane with the actin cytoskeleton through coiled coil-mediated trimeric coronin 1 molecules. *Mol. Biol. Cell* **16,** 2786–2798
21. Ferrari, G., Langen, H., Naito, M., and Pieters, J. (1999) A coat protein on phagosomes involved in the intracellular survival of mycobacteria. *Cell* **97,** 435–447
22. Yan, M., Di Ciano-Oliveira, C., Grinstein, S., and Trimble, W. S. (2007) Coronin function is required for chemotaxis and phagocytosis in human neutrophils. *J. Immunol.* **178,** 5769–5778
23. Yan, M., Collins, R. F., Grinstein, S., and Trimble, W. S. (2005) Coronin-1 function is required for phagosome formation. *Mol. Biol. Cell* **16,** 3077–3087
24. Song, H. D., Sun, X. J., Deng, M., Zhang, G. W., Zhou, Y., Wu, X. Y., Sheng,

Y., Chen, Y., Ruan, Z., Jiang, C. L., Fan, H. Y., Zon, L. I., Kanki, J. P., Liu, T. X., Look, A. T., and Chen, Z. (2004) Hematopoietic gene expression profile in zebrafish kidney marrow. *Proc. Natl. Acad. Sci. U.S.A.* **101,** 16240–16245

25. Jin, H., Sood, R., Xu, J., Zhen, F., English, M. A., Liu, P. P., and Wen, Z. (2009) Definitive hematopoietic stem/progenitor cells manifest distinct differentiation output in the zebrafish VDA and PBI. *Development* **136,** 647–654
26. Westerfield, M., Doerry, E., Kirkpatrick, A. E., and Douglas, S. A. (1999) Zebrafish informatics and the ZFIN database. *Methods Cell Biol.* **60,** 339–355
27. Jin, H., Xu, J., Qian, F., Du, L., Tan, C. Y., Lin, Z., Peng, J., and Wen, Z. (2006) The 5′ zebrafish scl promoter targets transcription to the brain, spinal cord, and hematopoietic and endothelial progenitors. *Dev. Dyn.* **235,** 60–67
28. Li, L., Jin, H., Xu, J., Shi, Y., and Wen, Z. (2011) Irf8 regulates macrophage *versus* neutrophil fate during zebrafish primitive myelopoiesis. *Blood* **117,** 1359–1369
29. Dobson, J. T., Da'as, S., McBride, E. R., and Berman, J. N. (2009) Fluorescence-activated cell sorting (FACS) of whole mount *in situ* hybridization (WISH) labeled hematopoietic cell populations in the zebrafish. *Br. J. Haematol.* **144,** 732–735
30. Qian, F., Zhen, F., Xu, J., Huang, M., Li, W., and Wen, Z. (2007) Distinct functions for different scl isoforms in zebrafish primitive and definitive hematopoiesis. *PLoS. Biol.* **5,** e132
31. Peri, F., and Nüsslein-Volhard, C. (2008) Live imaging of neuronal degradation by microglia reveals a role for v0-ATPase a1 in phagosomal fusion *in vivo*. *Cell* **133,** 916–927
32. Meijer, A. H., van der Sar, A. M., Cunha, C., Lamers, G. E., Laplante, M. A., Kikuta, H., Bitter, W., Becker, T. S., and Spaink, H. P. (2008) Identification and real-time imaging of a myc-expressing neutrophil population involved in inflammation and mycobacterial granuloma formation in zebrafish. *Dev. Comp Immunol.* **32,** 36–49
33. Herbomel, P., Thisse, B., and Thisse, C. (1999) Ontogeny and behavior of early macrophages in the zebrafish embryo. *Development* **126,** 3735–3745
34. Le Guyader, D., Redd, M. J., Colucci-Guyon, E., Murayama, E., Kissa, K., Briolat, V., Mordelet, E., Zapata, A., Shinomiya, H., and Herbomel, P. (2008) Origins and unconventional behavior of neutrophils in developing zebrafish. *Blood* **111,** 132–141
35. Traver, D., Paw, B. H., Poss, K. D., Penberthy, W. T., Lin, S., and Zon, L. I. (2003) Transplantation and *in vivo* imaging of multilineage engraftment in zebrafish bloodless mutants. *Nat. Immunol.* **4,** 1238–1246
36. Lieschke, G. J., Oates, A. C., Paw, B. H., Thompson, M. A., Hall, N. E., Ward, A. C., Ho, R. K., Zon, L. I., and Layton, J. E. (2002) Zebrafish SPI-1 (PU.1) marks a site of myeloid development independent of primitive erythropoiesis. Implications for axial patterning. *Dev. Biol.* **246,** 274–295
37. Lugo-Villarino, G., Balla, K. M., Stachura, D. L., Bañuelos, K., Werneck, M. B., and Traver, D. (2010) Identification of dendritic antigen-presenting cells in the zebrafish. *Proc. Natl. Acad. Sci. U.S.A.* **107,** 15850–15855
38. Niethammer, P., Grabher, C., Look, A. T., and Mitchison, T. J. (2009) A tissue-scale gradient of hydrogen peroxide mediates rapid wound detection in zebrafish. *Nature* **459,** 996–999
39. Zhang, Y., Bai, X. T., Zhu, K. Y., Jin, Y., Deng, M., Le, H. Y., Fu, Y. F., Chen, Y., Zhu, J., Look, A. T., Kanki, J., Chen, Z., Chen, S. J., Liu, T. X. (2008) *In vivo* interstitial migration of primitive macrophages mediated by JNK-matrix metalloproteinase 13 signaling in response to acute injury. *J. Immunol.* **181,** 2155–2164
40. Duffin, R., Leitch, A. E., Fox, S., Haslett, C., and Rossi, A. G. (2010) Targeting granulocyte apoptosis. Mechanisms, models, and therapies. *Immunol. Rev.* **236,** 28–40
41. Hallett, J. M., Leitch, A. E., Riley, N. A., Duffin, R., Haslett, C., and Rossi, A. G. (2008) Novel pharmacological strategies for driving inflammatory cell apoptosis and enhancing the resolution of inflammation. *Trends Pharmacol. Sci.* **29,** 250–257
42. Leitch, A. E., Duffin, R., Haslett, C., and Rossi, A. G. (2008) Relevance of granulocyte apoptosis to resolution of inflammation at the respiratory mucosa. *Mucosal Immunol.* **1,** 350–363
43. Jin, H., Li, L., Xu, J., Zhen, F. H., Zhu, L., Liu, P. P., Zhang, M., Zhang, W., and Wen, Z. L. (2012) Runx1 regulates embryonic myeloid fate choice in zebrafish through a negative feedback loop that confines Pu.1 expression. *Blood*, in press
44. Soehnlein, O., and Lindbom, L. (2010) Phagocyte partnership during the onset and resolution of inflammation. *Nat. Rev. Immunol.* **10,** 427–439
45. Nathan, C. (2006) Neutrophils and immunity. Challenges and opportunities. *Nat. Rev. Immunol.* **6,** 173–182
46. Dovi, J. V., He, L. K., and DiPietro, L. A. (2003) Accelerated wound closure in neutrophil-depleted mice. *J. Leukoc. Biol.* **73,** 448–455